Available online at www.elixirpublishers.com (Elixir International Journal)

Thermal Engineering

Elixir Thermal Engg. 162 (2022) 38706-38717

ISSN: 2229-712X

Simulation and Experimentation of Water Heating in a Metal Tube Placed in a Solar Collector

Boureima Kaboré[1,3], Germain Wende Pouiré Ouedraogo[2,3], Boukaré Ouedraogo[1,3], Salia Drabo[3], Sié Kam[3] and Dieudonné Joseph Bathiebo[3]

[1]UFR-ST, University Norbert ZONGO, Koudougou, Burkina Faso

[2]Higher School of Engineering (ESI), University of Fada N'Gourma, Fada N'Gourma, Burkina Faso

[3]Laboratory of Renewable Thermal Energies, University Joseph KI-ZERBO, Ouagadougou, Burkina Faso

ARTICLE INFO

Article history:
Received: 26 March 2022;
Received in revised form:
2 May 2022;
Accepted: 10 May 2022;

Keywords
Solar Exchanger,
Thermal Energy,
Solar Collector,
Water.

ABSTRACT

Our work relates to a numerical and experimental study of a solar exchanger designed and tested in Laboratory of Renewable Thermal Energy. This device is a unit for transforming solar radiation into thermal energy. The objective of our work is to study the evolution of temperature in the solar collector-water system. Our results show that this device makes it possible to heat the water during the day. The numerical results show that the temperature rise of the water is 47.84°C in March and 46.34°C in April.

1. Introduction

Heat exchangers are devices that allow the transfer of heat energy between two fluids separated by a solid surface [1]. In industrial processes, a large part of the thermal energy used passes through a heat exchanger at least once [2].

Several solar equipments available in our country have various applications such as drying, heating, refrigeration, cooking, power generation [3]. The variety of developed devices work with natural and forced convection flow [4, 5]. In this article, we wish to conduct a numerical and experimental study of a solar exchanger. This system consists of planar solar collectors whose role is to convert the incident radiant solar energy into thermal energy. This energy (heat) is then transferred to a heat transfer fluid (water) circulating inside a metal tube.

We will present the numerical and experimental results of thermal exchanges taking place inside the system.

2. Modeling of Solar Collector

The solar collector has the shape of a rectangular parallelepiped. It is covered with a window and surrounded by a wooden frame. Inside the sensor is a metal tube (Fig. 1).

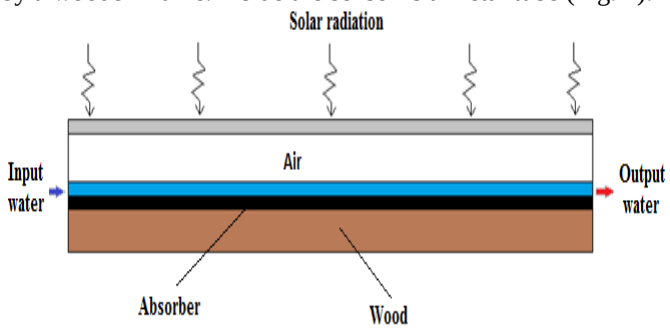

Figure 1. Diagram of solar collector

The role of this device is the heating of the water. Exposed to the sun, when the solar radiation arrives on the glazing of the sensor, part of the radiation passes through the window to reach the absorber. The latter heats up and transmits heat to the cold water that circulates inside the metal tube.

We use a one - dimensional model for conduction, convection and radiation exchanges. For modeling, we use the nodal method. This method consists of a fictitious spatial division of the system into "slices" of thicknesses whose sections are perpendicular to the direction of flow. In each slice, the homogeneous variables are assumed and the energy balances are written in successive time intervals until exhaustion of the duration of study. The transition from one slice to the next is carried out by retaining the output conditions of the "upstream" slice as input data of the "downstream" slice. For the discretization of the equations, we use the Finite Differences Method (Implicit Scheme) [4].

***Thermal balance in the solar collector**

-In the glazing :

$$e_v\rho_v c_{pv}\frac{dT_{VE}}{dt} = DFSA_V - h_{cae}(T_{VE}-T_{AE}) - h_{dv}(T_{VE}-T_{VI}) - h_{rvevc}(T_{VE}-T_{VC}) \quad (1)$$

$$e_v\rho_v c_{pv}\frac{dT_{VI}}{dt} = -h_{dv}(T_{VI}-T_{VE}) - h_{cacvi}(T_{VI}-T_{AC}) - h_{rvites}(T_{VI}-T_{TES}) \quad (2)$$

-In the air :

$$\frac{Vol_{ac}}{S_{ac}}\rho_a c_{pa}\frac{dT_{AC}}{dt} = -h_{cacvi}(T_{AC}-T_{VI}) - h_{cactes}(T_{AC}-T_{TES}) \quad (3)$$

-In the superior wall of the tube:

$$e_t\rho_t c_{pt}\frac{dT_{TES}}{dt} = -h_{cactes}(T_{TES}-T_{AC}) - h_{dt}(T_{TES}-T_{TIS}) - h_{rvites}(T_{TES}-T_{VI}) \quad (4)$$

$$e_t\rho_t c_{pt}\frac{dT_{TIS}}{dt} = -h_{dt}(T_{TIS}-T_{TES}) - h_{cetis}(T_{TIS}-T_E) \quad (5)$$

Tele:
E-mail address: kaboureim@gmail.com

-In the water:

$$\frac{Vol_e}{S_e}\rho_e c_{pe}\frac{dT_E}{dt} = -h_{cetis}(T_E - T_{TIS}) - h_{cetii}(T_E - T_{TII}) \quad (6)$$

-In the inferior wall of the tube:

$$e_t\rho_t c_{pt}\frac{dT_{TII}}{dt} = -h_{cetii}(T_{TII} - T_E) - h_{dt}(T_{TII} - T_{TEI}) \quad (7)$$

$$e_t\rho_t c_{pt}\frac{dT_{TEI}}{dt} = -h_{dt}(T_{TEI} - T_{TII}) - h_{dab}(T_{TEI} - T_{ABI}) \quad (8)$$

-In the absorber:

$$e_{ab}\rho_{ab}c_{pab}\frac{dT_{ABI}}{dt} = -h_{dab}(T_{ABI} - T_{TEI}) - h_{dab}(T_{ABI} - T_{ABE}) \quad (9)$$

$$e_{ab}\rho_{ab}c_{pab}\frac{dT_{ABE}}{dt} = -h_{dab}(T_{ABE} - T_{ABI}) - h_{db}(T_{ABE} - T_B) \quad (10)$$

***Determination of thermal transfer coefficients**

-The coefficient of convection between glazing and ambient air [6]:

$$h_{cae} = 2{,}8 + 3{,}3\times V_{ae} \quad (11)$$

Where: V_{ae} is ambient air velocity.

-Radiation between glazing and the vault of heaven:

$$h_{rvevc} = \frac{\sigma(T_{VE}^2 + T_{VC}^2)(T_{VE} + T_{VC})}{\frac{1-\varepsilon_v}{\varepsilon_v} + \frac{1}{F_{vevc}} + \frac{1-\varepsilon_{vc}}{\varepsilon_{vc}}\times\frac{s_v}{s_{vc}}} \quad (12)$$

With :

S_v, the surface of glazing and the surface of the vault of heaven.

$\varepsilon_{vc} = 1$: Emissivity of vault of heaven.

$F_{vevc} = 1$: Form factor between glazing and the vault of heaven.

We obtain equation (13) :

$$h_{rvevc} = \varepsilon_{ve}\sigma(T_{VE}^2 + T_{VC}^2)(T_{VE} + T_{VC}) \quad (13)$$

$\sigma = 5.67\times10^{-8} Wm^{-2}K^{-4}$ is Stefan-Boltzmann constant ;

T_{VE} is glazing temperature ;

$\varepsilon_v = 0.88$ is emissivity of glazing.

The temperature of vault of heaven is given by Swinbank expression [7]:

$$T_{vc} = 0.552\times T_{ae}^{1.5} \quad (14)$$

T_{ae} is the ambient air temperature.

-glazing coefficient of conduction [6]:

$$h_{dv} = \frac{\lambda_v}{e_v} \quad (15)$$

λ_v is glazing thermal conductivity et e_v is glazing thickness.

-Coefficient of natural convection of air in solar collector :

$$h_{cacvi} = \frac{Nu\times\lambda_a}{L} = \frac{0.6(Gr\,\mathrm{Pr})^{0.2}\times\lambda_a}{L} = \frac{0.6(0.7G\,\mathrm{r})^{0.2}\times\lambda_a}{L} \quad (16)$$

$$= \frac{0.6\left(0.7\times\frac{g\beta L^3|T_{AC} - T_{VI}|}{\nu^2}\right)^{0.2}\times\lambda_a}{L}$$

$$h_{cactes} = \frac{Nu\times\lambda_a}{L} = \frac{0.6(Gr\,\mathrm{Pr})^{0.2}\times\lambda_a}{L} = \frac{0.6(0.7G\,\mathrm{r})^{0.2}\times\lambda_a}{L} \quad (17)$$

$$= \frac{0.6\left(0.7\times\frac{g\beta L^3|T_{AC} - T_{TES}|}{\nu^2}\right)^{0.2}\times\lambda_a}{L}$$

With:

Nu, the number of Nusselt ;

λ_a, the thermal conductivity of air ;

L, the characteristic length of thermal exchange;

Gr, the number of Grashof ;

Pr, the number of Prandtl ;

g, the intensity of earthly gravity;

β, the air coefficient of dilation;

$\nu = 15.6\times10^{-6} m^2 s^{-1}$, the kinematic viscosity of the air;

T_{AC}, the air temperature in the collector ;

T_{VI}, temperature of the inner surface of glazing and

T_{TES}, temperature of outer superior surface of tube.

-Tube coefficient of conduction [3]:

$$h_{dt} = \frac{\lambda_t}{D_E\times\ln\left(\frac{D_E}{D_I}\right)} \quad (18)$$

If the tube is thin:

$$\ln\left(\frac{D_E}{D_I}\right) = \ln(1 + \frac{e_t}{D_I}) \to \frac{e_t}{D_I}$$

We obtain equation (19) :

$$h_{dt} = \frac{\lambda_t}{D_E\times\frac{e_t}{D_I}} \quad (19)$$

λ_{pt} is the thermal conductivity of the tube;

D_E is the outer diameter of the tube;

D_I is the inner diameter of the tube;

e_{pt} is the thickness of the tube.

Water coefficient of forced convection in the tube:

$$h_{ce} = \frac{Nu\times\lambda_e}{L} = \frac{(0.023\,\mathrm{Re}^{0.8}\times\mathrm{Pr}^n)\times\lambda_a}{L} \quad (20)$$

If there is cooling of water then $n = 0.3$; if there is heating of water then $n = 0.4$.

The characteristic length *L* is equal to the inside diameter D_I of the tube; λ_e is thermal conductivity of water ;

-Radiation coefficient between inner surface of glazing and outer superior surface of tube:

$$h_{rvites} = \frac{\sigma(T_{VI}^2 + T_{TES}^2)(T_{VI} + T_{TES})}{\frac{1-\varepsilon_v}{\varepsilon_v} + \frac{1}{F_{vites}} + \frac{1-\varepsilon_t}{\varepsilon_t}\times\frac{s_v}{s_t}} \quad (21)$$

with:

F_{vites}, form factor between inner surface of glazing and outer superior surface of tube;

ε_t, emissivity of tube ;

s_t, exchange surface of tube ;

T_{VI}, glazing inner surface temperature and T_{TES}, tube outer superior surface temperature.

-Conduction coefficient of absorber:

$$h_{dab} = \frac{\lambda_{ab}}{e_{ab}} \quad (22)$$

Conduction coefficient of wood:

$$h_{db} = \frac{\lambda_b}{e_b} \quad (23)$$

With :

λ_{ab} , thermal conductivity of absorber;

e_{ab} , absorber thickness ;

λ_b , thermal conductivity of wood and

e_b wood thickness.

For numerical simulation, we use an implicit finite difference method [8, 9]. The numerical resolution of the system of equations is done by the Gauss method. The calculation code used for the simulation is FORTRAN.

***Solar collector materials property**

Table 1 present physical and thermal property of solar collector materials.

Table 1. Physical and thermal property of solar collector material

Materials	Density (kg m^{-3})	Thermal conductivity (W m^{-1} K^{-1})	Thermal capacity (J kg^{-1} K^{-1})
Glazing	2530	0.78	840
Air	1.2	0.023	1006
Tube	7800	50	450
Water	1000	0.6	1460
Absorber	7800	50	450

3. Experimental device

Solar collector is 2.16 meters length and 1.16 meters wide.

Figure 2. Description of solar collector

The device consists of 4 plane sensors mounted in shunt. Each sensor is a parallelepiped box with a wooden frame. The upper face is a transparent glass which can be traversed by solar radiation. The side walls are thermally insulated with glass wool. Inside are serpentine tubes firmly fixed on a metal plate. This assembly (tube + metal plate) painted black forms the absorber. The sensors are placed directly horizontally on the roof of a level building. The heat transfer fluid (water) circulates inside the serpentine tubes.

The cold water that arrives at the sensors is divided into four parts. Thus, when a solar irradiation arrives on the glazing, a portion passes through the window to reach the absorber. The latter heats up and then transmits heat to the water flowing from the inlet to the outlet of the tubes.

Our experimental work consists in measuring, during the day, the global radiation and, on the other hand, the temperature of the water at the inlet of the sensor and that of the water at the outlet. Temperature measurements are performed using K-type thermocouples connected to a programmable temperature recorder (MIDI LOGGER GL 220). The radiation measurements are carried out with a pyranometer of type SR03.

The characteristics and metric properties of the sensor elements are given in Table 2.

Table 2. Characteristic of solar collector

	Glazing	Absorber	Wood
Thickness	$\delta_v = 5\,mm$	$\delta_a = 5mm$	$e_1 = 5\,cm$
Transmitivity	$\tau_v = 0.95$	-	
Emissivity	$\varepsilon_v = 0.88$	$\varepsilon_a = 0.95$	-
Reflectivity	$\rho_v = 0.05$	-	-
Absorptivity	-	$\alpha_a = 0.95$	-
Thermal conductivity	-	$\lambda_a = 386\,W/(m.K)$	-

4. Results and Discussion

4.1. Experimental results

The data recorded on 05/09/2016 and 05/01/2017, respectively, allowed to plot the evolution curves of the global radiation. We obtain the following Fig.3(a and b).

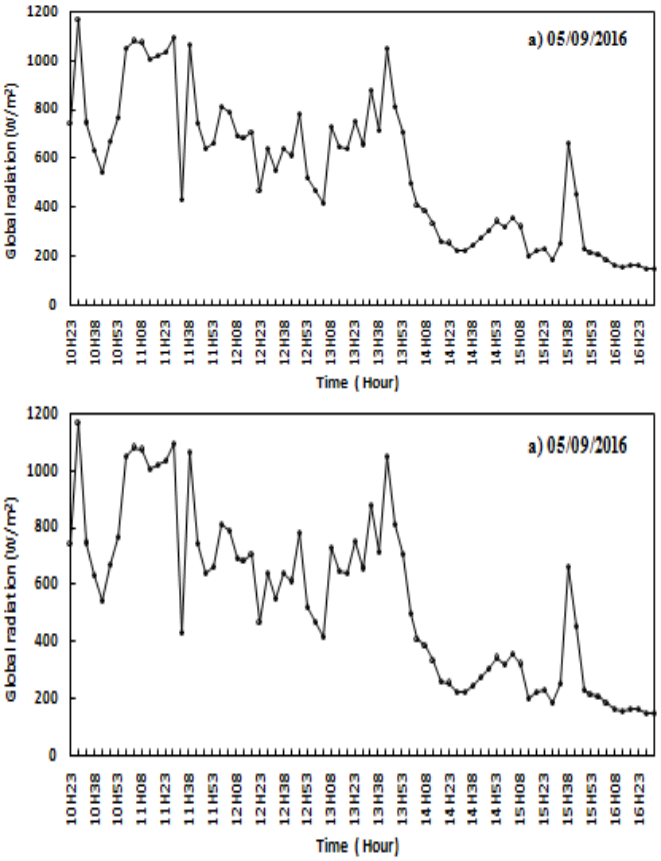

Figure 2. Global radiation on 05/09/2016 and 05/01/2017.

The day 05/09/2016 is a day with a cloudless skies and the day 05/01/2017 is cloudless. For the day of 05/09/2016, the observed fluctuations (Figure 3.a) are due to cloud passages. Nevertheless, it is during this day that we get a maximum value of 1170W/m² at 10h28min. This value is due to the clear sky without dust. For the day 05/01/2017, we obtain a bell curve (Figure 3.b) which shows a peak of 875 W/m² at 12h30min. The overall appearance of the curve of the radiation obtained is that of a Gaussian curve.

Fig. 4 shows the curves of the temperature of the water at the input (Te, e) of the sensor, temperature of the water at the output (Ts, e) and the temperature of the glazing (05/09/2016).

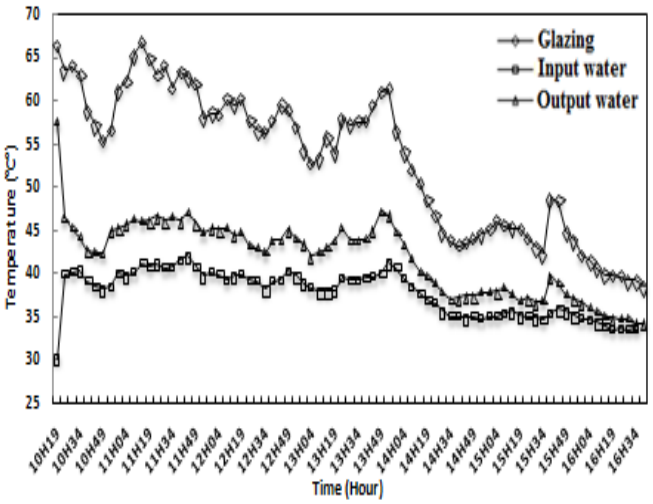

Figure 4. Evolution of temperatures on 05/09/2016

We observe in Fig. 4 that the curves of evolution of the temperatures of the water at the input and that of the water at the output of the collectors have the same appearance as that of the glazing. A temperature difference of about 5 °C is observed between the temperature of the input water and that of the output water. This difference decreases when the temperature of the glazing decreases. This is because the sensors do not store enough heat due to equipment failures (broken glazing, insufficient sealing). This does not favor the greenhouse effect.

Fig. 5 shows the curves of the temperature of the water at the input (Te, e) of the sensor, temperature of the water at the output (Ts, e) and the temperature of the glazing on (05/01/2017).

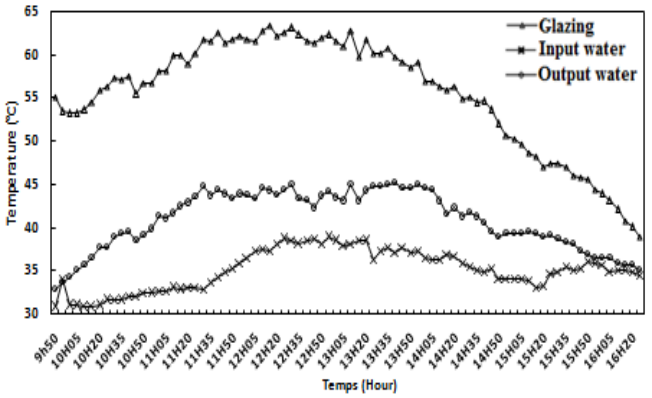

Figure 5. Evolution of temperatures on 05/01/2017.

We observe in Fig. 5 that the temperature of the water follows the same evolution as that of the glazing for the day of 05/01/17. A temperature difference of 11.1 °C between the temperature of the input water and that of the water at the output of the collectors is noted at 11h30min. This variation in temperature observed at the water level is explained by the fact that there is a transfer of heat from the absorber to the water. This deviation is retained as long as the incident radiation exists. As the temperature of the glazing decreases, the difference between the temperature of the input water and the temperature of the output water decreases. This shows that the decrease in global radiation also leads to a reduction in the thermal exchanges between the water and the absorber.

4.2. Numerical results

Fig. 6 presents evolution of temperatures in the collector on January.

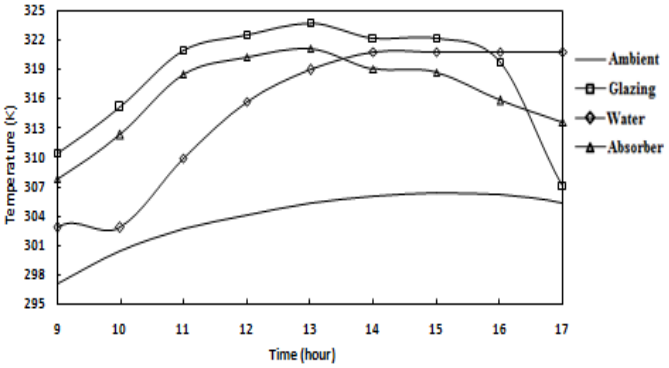

Figure. 6: Evolution of temperature in collector on January.

In Fig. 6, we observe that all temperatures increase between 9h and 13h. From 1 pm, the temperature changes become different. The temperature of the glazing and that of the absorber have the same appearance. Over time, the temperature of the glazing is higher than that of the absorber. Beyond 1 pm, there is a decrease in the temperature of the glazing and that of the absorber. This is due to the lowering of the ambient temperature (or the decrease of the solar radiation). As for the temperature of the water, it increases from 9h (302.88 K) to 14h (320.94 K), and then stabilizes until 17h. This shows that the temperature rise of the water from 9 am to 5 pm is 18.06 K. During the month of January, the absorber heats less than the glazing and does not promote a good heat exchange between the absorber and the water. Thus, the heating of the water is less important.

Fig. 7 presents evolution of temperatures in the collector on March.

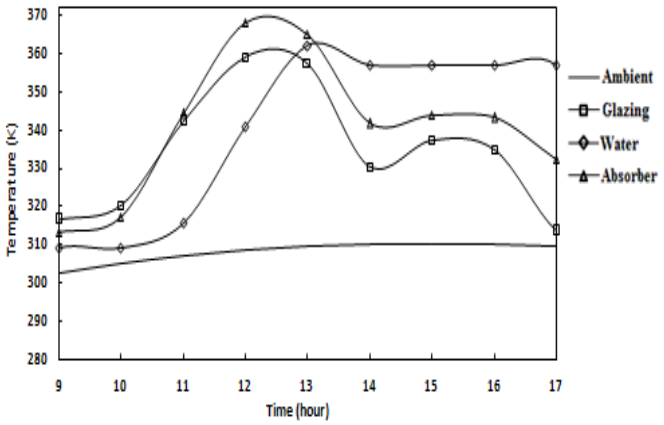

Figure 7. Evolution of temperatures in collector on march

In Fig. 7, we observe that the temperature of the glazing and that of the absorber have the same pace. Over time, the temperature of the absorber is higher than that of the glazing. The maximum temperatures of glazing and absorber are reached at 12:00 and are respectively 359.27K and 368.15K. The temperature of the water increases during the day and reached its maximum value (365.24K) at 13.00. From 1:00 pm, the temperature of the water decreases slightly until reaching 357,12K at 17h00. From 9 am to 5 pm, the rise of temperature is 47.84K.

The following Fig. 8 shows the evolution of the temperatures in the collector during April.

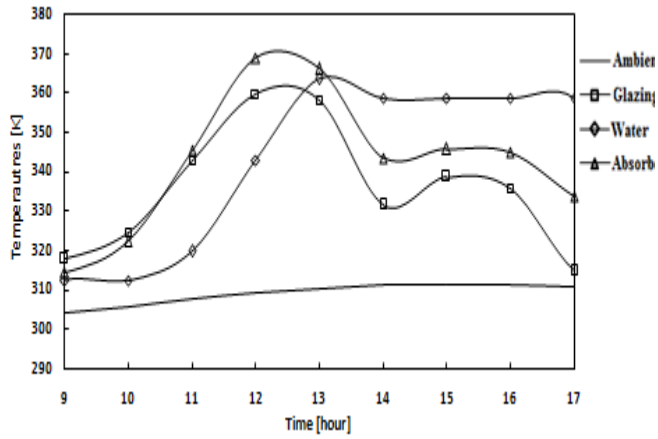

Figure 3. Evolution of temperatures in collector on April

In Fig. 8, we observe that the temperature curves have the same characteristics as those of Fig. 7. Over time, the temperature of the absorber is higher than that of the glazing. The maximum temperatures of glazing and absorber are reached at 12h00 and are respectively 359.87K and 368.97K. The temperature of the water increases during the day and reaches its maximum value (363.52K) at 13h00. Starting at 1pm, the water temperature decreases slightly to 358.67K at 17h00. From 9h00 to 17h00, the temperature rise is 46.34K.

Table 3 below shows the minimum and maximum water temperature in January, in the cases of the experiment and the simulation (Fig. 5 and Fig. 6).

Table 3. Minimum and maximum water temperature in January

Case	Minimum temperature of water	Maximum temperature of water
Experience	307.10 K	318.10 K
Simulation	302.88 K	319.04 K

Table 3 shows that experimentally, the rise in water temperature is 11K (or 11 °C) in January. While numerically, this value is 16.16 K (or 16.16 °C). The difference between the numerical and the experimental results can be explained by the fact that the experimental sensors do not store enough heat because of the hardware failures.

Conclusion

In this paper, we conducted a numerical and experimental study of a solar exchanger. For modeling, we used the nodal method and the implicit finite difference method. The computer program is executed using the FORTRAN calculation code.

This work allowed to evaluate the elevation of the temperature of the water flowing inside a tube placed in a flat solar collector. The experimental results show that the reduction of the global radiation leads to a reduction of the thermal exchanges between the water and the absorber. The temperature rise of the water is 11 °C in the case of the experiment. In the simulation case, the temperature rise is 16.16 °C. The difference between the numerical and experimental results can be explained by the fact that the experimental sensors do not store enough heat due to equipment failures (broken glazing and leakage problem).

References

[1] A. M. Bianchi, Yves Fautrelle, Jacqueline Etay, Transferts thermiques, Livre, Agence universitaire de la Francophonie, Lausanne, 550 p., 2004.

[2] A. Bontemps, Alain Garrigue, Charles Goubier, Jacques Huetz, Christophe Marvillet, Pierre MERCIER, Roland VIDIL, Echangeur de chaleur, Description des échangeurs, Editions : Techniques de l'Ingénieur, Traité Génie énergétique.

[3] Germain W. P. OUEDRAOGO, étude numérique et expérimentale de l'écoulement de l'air en convection naturelle dans une tour solaire : application au séchage du gombo, Thèse de Doctorat Unique, Ouagadougou, Juillet 2017.

[4] M. N'DONGO, Etude théorique d'un générateur solaire d'air chaud constitué d'une serre agricole et d'un stockage de chaleur en sous-sol à l'aide de conduits. Application au séchage, Thèse de Doctorat de 3ème cycle, Université Blaise Pascal, France, 1989.

[5] A.E. Kabeel, M.H. Hamed, Z.M. Omara, A.W. Kandeal, Solar air heaters: Design configurations, improvement methods and applications – A detailed review, Renew. Sustain. Energy Rev. 70 (2017) 1189–1206, https://doi.org/10.1016/j. rser.2016.12.021.

[6] A. Famiglietti, A. Lecuona, Direct solar air heating inside small-scale linear Fresnel collector assisted by a turbocharger: Experimental characterization, Applied Thermal Engineering 196(2021)117323.

[7] A. Fudholi, K. Sopian, M. H. Ruslan, M. Y. Othman and M. Yahya, Thermal Efficiency of Double Pass Solar Collector with Longitudinal Fins Absorbers, Article, American Journal of Applied Sciences 8 (3) (2011).

[8] B. Carnahan, H. A. Lither and J. O. Wilkes, Applied Numerical Methods, P J. Wiley and sons. Inc, New York, 1969.

[9] E.F. Nogotov, B.M. Berkovsky and W.J. Minkowycz, Application of Numerical Heat Transfer, Mc Graw Hill Book Company, New York, 1978.